Narrowband Interferers Cancellation versus Estimation: Impact on Synchrophasor Measurement

Xuansheng Shan[1,2], David Macii[2], He Wen[1], Dario Petri[2]
[1]*Hunan University - College of Electrical and Information Engineering,* Changsha, P.R. China
[2]*University of Trento - Dep. of Industrial Engineering*, Trento, Italy
E-mail: shanxs006@hnu.edu.cn, {david.macii, dario.petri}@unitn.it, he_wen82@126.com

***Abstract* — One of the open issues in Phasor Measurement Units (PMU) design is how to suppress the influence of harmonics and Out-of-Band Interharmonics (OOBIs) on synchrophasor measurement over short observation intervals. In most PMUs, such narrowband interferers are removed before or during synchrophasor estimation. However, several researchers noticed that estimating harmonics and/or OOBIs is beneficial not only to extract more information from the acquired signal, but also to indirectly improve the estimation accuracy of the parameters of the fundamental component. At the moment, the pros and cons of these two opposite approaches are not fully clear, mainly due to the difficulty to draw general and fair conclusions from the comparison of different algorithms. In this paper, we partially address this problem by comparing two algorithms that rely on both a common theoretical background and the same final estimation stage, i.e., the Whitening-based Tuned Interpolated Dynamic Discrete Fourier Transform (WTpD2FT) and the Enhanced Interpolated Dynamic Discrete Fourier Transform (eIpD2FT). The former algorithm attempts to transform narrowband disturbances into white noise, whereas the latter detects and estimates the parameters just of the most significant interferers. Several simulation results suggest that the estimation of the narrowband interferers' parameters generally returns high-accuracy values of synchrophasor, fundamental frequency and rate of change of frequency (ROCOF) especially when large OOBIs affect the fundamental component, whereas the whitening-based disturbance cancellation approach is slightly preferable in the presence of multiple harmonics and growing noise levels.**

***Keywords*—Phasor Measurement Unit (PMU), harmonics and interharmonics, ESPRIT, Interpolated Dynamic Discrete Fourier Transform (IpD2FT).**

I. INTRODUCTION

Low-order harmonics and out-of-band inter-harmonics (OOBIs) are notoriously the most critical interferers affecting the accuracy of Phasor Measurement Units (PMU). Since PMUs were primarily conceived to perform UTC-synchronized measurements of amplitude, phase, frequency and rate of change of frequency (ROCOF) of the AC fundamental component only, most of the existing devices are designed to attenuate the narrowband interferers (e.g., through digital filters) before or during the estimation of the quantities of interest. This is for instance the default approach described in Annex D of the IEEE/IEC Standard 60255-118-1:2018 where the in-phase and quadrature components of the digitized 50 Hz or 60 Hz signal are down-converted around 0 Hz, while harmonics and Out-of-Band Interharmonics (OOBI) are filtered in parallel by two identical digital filters [1]. A key feature of this approach is the selectivity of such filters, while keeping their impulse response (and the corresponding group delay) as short as possible. In this regard, the filter design criteria are of paramount importance [2]. Several techniques have been proposed to improve filter selectivity compared with the examples reported in the IEC/IEEE Standard, e.g., by using least-squares optimization techniques [3], by cascading adaptive filters with the notches of the frequency response tuned at harmonic frequencies [4], or through optimal filter banks resulting from convex semi-infinite programming [5].

An alternative to digital filtering is provided by the whitening techniques, i.e., linear transformations that turn narrowband interferers into white noise, thus mitigating their effect on the fundamental component [6]. For instance, a two-stage whitening transform with off-nominal frequency estimation and correction was successfully applied before a Taylor-Kalman Filter to increase synchrophasor estimation accuracy over very short observation intervals [7]. A similar whitening technique with both preliminary frequency estimation and observation interval adjustment will be also adopted in this paper to evaluate its impact on the Interpolated Dynamic Discrete Fourier Transform (IpD2FT) estimator [8]. In the following, this new algorithm will be referred to as Whitening-based Tuned IpD2FT (WTIpD2FT) algorithm.

Over the last few years, several researchers suggested a different approach to mitigate the effect of narrowband interferers, which relies on the estimation of interferers' parameters (regarded as a part of the signal model) instead of disturbance filtering. The main drawback of these approaches is twofold: i) the computational burden grows as a function of the number of parameters to be estimated; ii) the number of narrowband components is usually unknown a priori and has to be established. Also, if one or more disturbances are not detected, estimation accuracy may be degraded.

The Taylor-Fourier Transform (TFT) is a renowned algorithm for PMUs, conceived to estimate the parameters of a given number of harmonics [9]. It builds upon the Taylor's series expansion (truncated to a given order) of the dynamic phasors of the narrowband components included in the model. Recently, the TFT was further enhanced when three-phase signals are considered [11]. However, the standard TFT cannot include the OOBIs in the model and the number of harmonics is unknown a priori. Also, the TFT estimation accuracy degrades when the fundamental frequency differs significantly from the nominal value. A variety of methods can be used to tackle this problem, e.g., through a preliminary estimation of the frequency of one or more narrowband components. For instance, the Interpolated Discrete Time Fourier Transform (IpDFT) [12], the Estimation of Signal Parameters via Rotational Invariant Techniques (ESPRIT) [13], or the matrix pencil method can be used [14]. Of course, selecting an incorrect model order can significantly

deteriorate TFT estimation accuracy, and in any case the problem of OOBI detection persists. This problem can be tackled either by using a Compressive Sensing Taylor-Fourier Multifrequency Technique [15] (recently extended for harmonics estimation, too [16]), or by applying the IpDFT iteratively to estimate and to compensate for the effect of the spectral leakage caused by the narrowband interferers exceeding a given heuristic threshold [17].

Due to the inherent differences between the various algorithms described above, it is hard to draw general conclusions on whether (and to what extent) it is better to remove the narrowband interferers or to estimate their parameters. This paper presents a first step to address this issue through a fair side-by-side comparison between two alternative algorithms based on the very same theoretical background and the same final estimation stage, i.e., the Whitening-based Tuned Interpolated Dynamic Discrete Fourier Transform (WTIpD2FT) and the Enhanced Interpolated Dynamic Discrete Fourier Transform (eIpD2FT) [18]. Both algorithms rely on the Singular Value Decomposition (SVD) of the signal autocorrelation matrix, followed by a preliminary ESPRIT stage to estimate the frequency of one or more narrowband components and a final IpD2FT estimator. However, the WTIpD2FT algorithm is based on the same idea as the solution presented in [7], i.e., it relies on a two-stage narrowband interferers whitening, so that only the fundamental synchrophasor is returned by the final IpD2FT estimator. On the contrary, the eIpD2FT algorithm exploits a detector based on an adaptive threshold that is used to determine the number of significant harmonics and OOBIs components, whose parameters are returned by the cascade of the ESPRIT and the expanded IpD2FT estimators [18]

The rest of the paper is organized as follows. In Section II, the signal model and the theoretical background of the WTIpD2FT and the eIpD2FT algorithms is described. In Section III, the results of several simulations performed are reported and compared. Finally, Section IV concludes the paper.

II. Algorithms Description

The discrete-time sequence obtained by sampling the AC signal at the input of a PMU channel with frequency $f_s = Mf_0$ where M is an integer number and f_0 is the nominal fundamental frequency (i.e., 50 Hz or 60 Hz) is:

$$x(n) = \sum_{d=1}^{D} A_d(n)\cos\left(2\pi \frac{f_d}{f_s} n + \varphi_d(n)\right) + \varepsilon(n) \qquad (1)$$

where $A_d(n)$, f_d and $\varphi_d(n)$ are the amplitude, the static frequency and the instant phase (at a given sampling time n/f_s) of the dth narrowband component (for d=1,…,D) of the acquired signal, while $\varepsilon(n)$ is the almost white noise floor with zero-mean and variance σ^2.

Note that $d = 1$ represents the fundamental component (whose synchrophasor magnitude and phase, frequency and ROCOF must be measured by the PMU) whereas all the other components (i.e., for $d = 2,\ldots,D$) can be regarded as interferers. Therefore, either they can be filtered out (that is the default PMU approach) or their parameters can be estimated by the PMU algorithm. It is worth emphasizing that, as briefly explained in Section I, the number of interferers emerging significantly from the noise floor is unknown a priori. Therefore, the value of D must be properly determined at run-time, which is a well-known problem [19], [20]. Let $\boldsymbol{y}(n) = [x(n)\ \ x(n+1)\ \ \ldots\ \ x(n+N-1)]^{\mathrm{T}}$ be an N-long column vector of signal samples (with $N > 2D$). If L data records shifted by $1 \le R \le N$ samples at a time are collected, the autocorrelation matrix Q of $\boldsymbol{y}(n)$, i.e., $Q = E\{\boldsymbol{y}(n)\boldsymbol{y}^{\mathrm{T}}(n)\}$ (where $E\{\cdot\}$ is the expectation operator), can be estimated and decomposed into singular values, as follows [21]:

$$\hat{Q} = \frac{1}{L}\sum_{l=1}^{L} \boldsymbol{y}(n-l\cdot R)\boldsymbol{y}^{\mathrm{T}}(n-l\cdot R) = \begin{bmatrix}\hat{U}_{\mathrm{fun}} & \hat{\bar{U}}_{\mathrm{fun}}\end{bmatrix}\begin{bmatrix}\hat{\Lambda}_{\mathrm{fun}} & 0\\ 0 & \hat{\bar{\Lambda}}_{\mathrm{fun}}\end{bmatrix}\begin{bmatrix}\hat{U}_{\mathrm{fun}}^{\mathrm{T}}\\ \hat{\bar{U}}_{\mathrm{fun}}^{\mathrm{T}}\end{bmatrix} =$$
$$= \begin{bmatrix}\hat{U}_{\mathrm{fun}} & \hat{U}_{\mathrm{int}} & \hat{U}_{\mathrm{noise}}\end{bmatrix}\begin{bmatrix}\hat{\Lambda}_{\mathrm{fun}} & 0 & 0\\ 0 & \hat{\Lambda}_{\mathrm{int}} & 0\\ 0 & 0 & \hat{\Lambda}_{\mathrm{noise}}\end{bmatrix}\begin{bmatrix}\hat{U}_{\mathrm{fun}}^{\mathrm{T}}\\ \hat{U}_{\mathrm{int}}^{\mathrm{T}}\\ \hat{U}_{\mathrm{noise}}^{\mathrm{T}}\end{bmatrix} \qquad (2)$$

where:

- the "hat" symbol (both here and in the following) denotes the estimated quantities;
- $\hat{\Lambda}_{\mathrm{fun}}$ and $\hat{\bar{\Lambda}}_{\mathrm{fun}}$ are the 2×2 and $(2D-2)\times(2D-2)$ diagonal sub-matrices including the singular values associated with the fundamental component and all the other signal components, respectively;
- $\hat{U}_{\mathrm{fun}}$ and $\hat{\bar{U}}_{\mathrm{fun}}$ are $N\times 2$ and $N\times(N-2)$ matrices, whose columns are the corresponding estimated singular vectors.

Observe that $\hat{\bar{\Lambda}}_{\mathrm{fun}}$ and $\hat{U}_{\mathrm{noise}}$ can be further partitioned as $\hat{\bar{\Lambda}}_{\mathrm{fun}} = \mathrm{diag}(\hat{\Lambda}_{\mathrm{int}}, \hat{\Lambda}_{\mathrm{noise}})$ and $\hat{\bar{U}}_{\mathrm{fun}} = \begin{bmatrix}\hat{U}_{\mathrm{int}} & \hat{U}_{\mathrm{noise}}\end{bmatrix}$, to separate the singular values and vectors associated with the narrowband interferers from those of the wideband noise vector subspace.

In the case at hand, both the WTIpD2FT and the eIpD2FT algorithms estimate the Q matrix and apply (2) in a slightly different way, as it will be explained more in detail in the following subsections. The simplified block diagrams of both estimation algorithms are shown in Fig. 1.

A. WTIpD2FT description

In the WTIpD2FT case, the Q matrix is initially estimated through (2), with $L = N = C\cdot M$ (where C is the number of nominal cycles in each observation interval) and $R = 1$ (i.e., the records are shifted sample-by-sample). This value of R is needed both to sweep uniformly the phase angles of all narrowband components within [0, 2π] and to keep the algorithm delay within reasonable limits. The singular vectors and values of $\hat{Q}$ other than those of the fundamental component can be used to compute the so-called whitening matrix [6]:

$$S = \begin{bmatrix}\hat{U}_{\mathrm{fun}} & \hat{\bar{U}}_{\mathrm{fun}}\end{bmatrix}\begin{bmatrix}I_2 & 0\\ 0 & \sigma_\varepsilon \hat{\bar{\Lambda}}_{\mathrm{fun}}^{-\frac{1}{2}}\end{bmatrix}\begin{bmatrix}\hat{U}_{\mathrm{fun}}^{\mathrm{T}}\\ \hat{\bar{U}}_{\mathrm{fun}}^{\mathrm{T}}\end{bmatrix}, \qquad (3)$$

where I_2 is the 2×2 identity matrix and σ_ε is the standard deviation of the zero-mean artificial wideband noise floor that is used to replace the singular values associated with both the

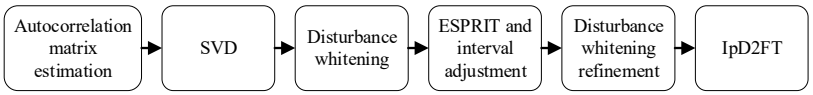

(a) WTIpD2FT

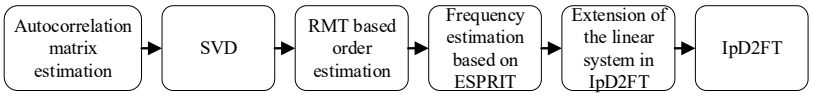

(b) eIpD2FT

Fig. 1. Block diagrams of two alternative algorithms for synchrophasor estimation. They are both based on: i) the singular-value decomposition of the autocorrelation matrix of the collected signal, ii) the ESPRIT algorithm for a preliminary estimation of the fundamental frequency of one or more narrowband components, and iii) a final IpD2FT-based synchrophasor estimation stage. The WTIpD2FT algorithm (a) is designed to attenuate all narrowband interferers through a whitening transformation. The eIpD2FT algorithm (b) relies instead on a detector with an adaptive threshold to determine the most significant narrowband components in the signal, whose parameters are then estimated by an extended version of the IpD2FT algorithm.

narrowband interferers and the original acquisition noise. Matrix (3) is indeed used to perform a linear transformation of the most recent N-long data samples,

$$\boldsymbol{y}_S(n) = S\,\boldsymbol{y}(n). \tag{4}$$

As shown in [6], the spectrum of $\boldsymbol{y}_S(n)$ exhibits a lower harmonic and interharmonic content than $\boldsymbol{y}(n)$. Moreover, the spectral purity of the signal can be further enhanced if an integer number of fundamental cycles is acquired [7]. For this reason, the data record length N can refined as follows: $\hat{N} = \left\lfloor \frac{N}{1+\hat{\delta}} \right\rfloor$ or $\hat{N} = \left\lfloor \frac{N}{1+\hat{\delta}} \right\rfloor + 1$ (depending on whether $\left\lfloor \frac{N}{1+\hat{\delta}} \right\rfloor$ is odd or even) where $\lfloor \cdot \rceil$ is the "rounding to the nearest integer" operator and $\hat{\delta} = \frac{\hat{f}_1 - f_0}{f_0}$ is the estimated fractional frequency offset. The frequency offset can be estimated in a variety of ways, but in this paper the ESPRIT technique is used to ensure a fair comparison with the eIpD2FT algorithm [18]. In particular, assuming that the no other narrowband components than the fundamental are significant after the first whitening step, then $\hat{f}_1 = \frac{\hat{\omega}_1}{2\pi} f_s$ where $\hat{\omega}_1$ is the positive exponent of one of the two complex conjugate eigenvalues of the 2×2 rotation matrix resulting from [21]

$$\hat{\boldsymbol{\Psi}}_1 = \left(\hat{U}_{\text{fun}_1}^{\mathrm{T}} \hat{U}_{\text{fun}_1}\right)^{-1} \hat{U}_{\text{fun}_1}^{T} \hat{U}_{\text{fun}_2}, \tag{5}$$

where $\hat{U}_{\text{fun}_1} = \begin{bmatrix} I_{N-1} & \mathbf{0} \end{bmatrix} \hat{U}_{\text{fun}}$ and $\hat{U}_{\text{fun}_2} = \begin{bmatrix} \mathbf{0} & I_{N-1} \end{bmatrix} \hat{U}_{\text{fun}}$.

Once $\hat{N}$ is computed, expressions (3) and (4) are applied again to the input data record over $\hat{N}$ samples. The resulting, doubly whitened data record (denoted as $\boldsymbol{y}_S'(n)$ in the following) is finally applied to the classic IpD2FT estimator described in [8]. In particular, by equating the spectral samples of $\boldsymbol{y}_S'(n)$ (obtained using the Hann window) and the threoretical Discrete-Time Fourier Transform (DTFT) of the fundamental synchrophasor's Taylor series truncated to the second-order, it follows that

$$\begin{bmatrix} \hat{\boldsymbol{p}} \\ \hat{\boldsymbol{p}}^* \end{bmatrix} = \begin{bmatrix} W_P(\hat{\nu}_1) & W_I(\hat{\nu}_1) \\ W_I^*(\hat{\nu}_1) & W_P^*(\hat{\nu}_1) \end{bmatrix}^{-1} \begin{bmatrix} \boldsymbol{Y}_s' \\ \boldsymbol{Y}_s'^* \end{bmatrix}, \tag{6}$$

where symbol * denotes the complex conjugate operator and

- $\hat{\boldsymbol{p}} = \begin{bmatrix} \hat{p}_{1,0} & \hat{p}_{1,1} & \hat{p}_{1,2} \end{bmatrix}^{\mathrm{T}}$ is the vector with the 0th-, 1st-, and 2nd-order coefficients of the Taylor's series of the fundamental synchrophasor;
- $\boldsymbol{Y}_s' = \begin{bmatrix} Y_s'(\hat{\nu}_1 - 1) & Y_s'(\hat{\nu}_1) & Y_s'(\hat{\nu}_1 + 1) \end{bmatrix}^{\mathrm{T}}$ is the column vector including: the DTFT value of $\boldsymbol{y}_S'(n)$ at the estimated frequency of the fundamental expressed in bins (i.e., for $\hat{\nu}_1 = \frac{\hat{\omega}_1}{2\pi\hat{N}}$) and the two closest spectral samples (namely at a distance of ±1 bin from the fundamental).
- Finally, $W_P(\hat{\nu}_1)$ and $W_I(\hat{\nu}_1)$ are defined as:

$$W_P(\hat{\nu}_1) = \begin{bmatrix} W_0(-1) & W_1(-1) & W_2(-1) \\ W_0(0) & W_1(0) & W_2(0) \\ W_0(1) & W_0(1) & W_2(1) \end{bmatrix}, \tag{7}$$

$$W_I(\hat{\nu}_1) = \begin{bmatrix} W_0(2\hat{\nu}_1 - 1) & W_1(2\hat{\nu}_1 - 1) & W_2(2\hat{\nu}_1 - 1) \\ W_0(2\hat{\nu}_1) & W_1(2\hat{\nu}_1) & W_0(2\hat{\nu}_1) \\ W_0(2\hat{\nu}_1 + 1) & W_1(2\hat{\nu}_1 + 1) & W_2(2\hat{\nu}_1 + 1) \end{bmatrix}, \tag{8}$$

where $W_k(\nu)$ denotes the kth derivative of the DTFT of the chosen window function $w(n)$, i.e., [8]

$$W_k(\nu) = \frac{1}{W_0(0)} \sum_{n=-\frac{\hat{N}-1}{2}}^{\frac{\hat{N}-1}{2}} n^k w(n) e^{-j\frac{2\pi}{\hat{N}}\nu n} = \frac{j^k}{W_0(0)} \frac{d^k W}{d\omega^k}\bigg|_{\frac{2\pi}{\hat{N}}\nu}. \tag{9}$$

Ultimately, the fundamental synchrophasor in the center of each observation interval is $\hat{p}_{1,0}$, while the corresponding values of frequency and ROCOF are given by [10]

$$\hat{f}_1 = \frac{f_s}{2\pi} \frac{\mathrm{Im}\left\{\hat{p}_{1,1}\hat{p}_{1,0}^*\right\}}{\left|\hat{p}_{1,0}\right|^2} + f_0, \tag{10}$$

$$\mathrm{ROCOF} = \frac{f_s^2}{\pi}\left[\frac{\mathrm{Im}\left\{\hat{p}_{1,2}\hat{p}_{1,0}^*\right\}}{\left|\hat{p}_{1,0}\right|^2} - \frac{\mathrm{Re}\left\{\hat{p}_{1,1}\hat{p}_{1,0}^*\right\}\mathrm{Im}\left\{\hat{p}_{1,1}\hat{p}_{1,0}^*\right\}}{\left|\hat{p}_{1,0}\right|^4}\right]. \tag{11}$$

To further reduce the impact of wideband noise, the frequency and ROCOF values computed sample-by-sample are averaged over one reporting period.

B. eIpD2FT description

In the eIpD2FT case, the estimation of the autocorrelation matrix Q and the subsequent SVD in (2) are used to

implement a detector, based on Random Matrix Theory (RMT), of the most significant narrowband interferers(i.e., the *D* value). This detector relies on an iterative hypothesis test. In particular, the threshold identifying the greatest estimated singular value associated with the noise subspace is computed adaptively, so that the probability of wrongly regarding a noise component as a narrowband interferer converges to a given value. The details of the detection algorithm are reported in [18]. It is worth emphasizing that, the following conditions must be applied when computing (2), i.e.

1. Nonoverlapped data records must be considered (i.e., $R = N$), otherwise the theoretical expressions underlying the RMT-based method are no longer valid;
2. The value of frequency f_s/N must not coincide with the frequency of the fundamental, of one of its harmonics or of any OOBI specified within the IEEE/IEC bands. This condition ensures that the initial phase angles of the *D* narrowband components in *L* data records are swept quite uniformly within [0, 2π], if *L* is large enough.
3. The value of the ratio *N/L* should result from the tradeoff between the acquisition delay and the asymptotic limit for narrowband component detection, which is approximately $\sigma^2\sqrt{N/L}$ [22].

The three conditions above can be met if $L = R = N = \left[f_s/37.5+1\right]$, where again $[\cdot]$ is the rounding operator.

After the number of narrowband components is computed, their frequencies can be estimated through ESPRIT, by simply extending the approach explained in Section II.A. In particular, denoting $\hat{U}_D = \left[\hat{U}_{\text{fun}} \quad \hat{U}_{\text{int}}\right]$, the frequency estimates of the detected narrowband components are $\hat{f}_d = \frac{\hat{\omega}_d}{2\pi} f_s$, for $d = 1,\ldots, \hat{D}$, where $\hat{\omega}_d$ is the positive exponent of the *d*th eigenvalue of the rotation matrix given by

$$\hat{\Psi}_D = \left(\hat{U}_{D_1}^{\mathrm{T}}\hat{U}_{D_1}\right)^{-1}\hat{U}_{D_1}^{\mathrm{T}}\hat{U}_{D_2}. \tag{12}$$

where $\hat{U}_{D_1} = \left[I_{N-1} \quad \mathbf{0}\right]\hat{U}_D$ and $\hat{U}_{D_2} = \left[\mathbf{0} \quad I_{N-1}\right]\hat{U}_D$.

To limit the overall estimation latency, the IpD2FT-based final estimator runs in parallel to the narrowband components detector and the ESPRIT algorithm [18]. As a consequence, the observation interval length adopted by the IpD2FT estimator can be different from *N* and it is set to $\hat{N} = \left\lfloor \frac{C \cdot M}{1+\hat{\delta}} \right\rfloor$ or $\hat{N} = \left\lfloor \frac{C \cdot M}{1+\hat{\delta}} \right\rfloor + 1$ to enable a fair comparison with the WTIpD2FT at the same reference times. The IpD2FT formulation was extended by including in the model all the spectral lines associated with the $\hat{D}$ detected narrowband components and assuming that only the static (i.e., zero order) components of the interferers are considered. Thus, if $\hat{\mathbf{v}} = \left[\hat{v}_1 \quad \cdots \quad \hat{v}_{\hat{D}}\right]^{\mathrm{T}}$ is the vector of narrowband components' frequency expressed in frequency bins, $\hat{\boldsymbol{p}} = \left[\hat{p}_{1,0} \quad \hat{p}_{1,1} \quad \hat{p}_{1,2} \quad \hat{p}_{2,0} \quad \cdots \quad \hat{p}_{\hat{D},0}\right]^{\mathrm{T}}$ is the vector of all unknown phasor coefficients to be estimated, and $\boldsymbol{Y}' = \left[Y'(\hat{v}_1-1) \quad Y'(\hat{v}_1) \quad Y'(\hat{v}_1+1) \quad Y'(\hat{v}_2) \quad \cdots \quad Y'(\hat{v}_D)\right]^{\mathrm{T}}$ is the vector of the windowed DTFT values of the $\hat{N}-$long data vector $\boldsymbol{y}'(n)$ at the considered frequency bins (note that $\boldsymbol{y}'(n)$ is different from $\boldsymbol{y}_S'(n)$ since no whitening is applied in the present estimator), it results that:

$$\begin{bmatrix} \hat{\boldsymbol{p}} \\ \hat{\boldsymbol{p}}^* \end{bmatrix} = \begin{bmatrix} W_P(\hat{\mathbf{v}}) & W_I(\hat{\mathbf{v}}) \\ W_I^*(\hat{\mathbf{v}}) & W_P^*(\hat{\mathbf{v}}) \end{bmatrix}^{-1} \begin{bmatrix} \boldsymbol{Y}' \\ \boldsymbol{Y}'^* \end{bmatrix}, \tag{13}$$

where matrices $W_P(\hat{\mathbf{v}})$ and $W_I(\hat{\mathbf{v}})$ are similar to (13) and (14), but they have a greater size (i.e., $\left(\hat{D}+2\right)\times\left(\hat{D}+2\right)$). So, they are omitted for space constraints, but can be found in [18]. Of course, also in this case the estimated value of the fundamental synchrophasor is $\hat{p}_{1,0}$, while the dynamic frequency and ROCOF are again given by (10) and (11).

III. Simulation Results

The performances of the WTIpD2FT and the eIpD2FT algorithms are analyzed and compared in different scenarios. The first scenario is under some of the most critical *M Class* testing conditions described in the IEEE/IEC Standard 60255-118-1:2018 [1]. In the second scenario, the effect of critical off-nominal frequency deviations and multiple harmonics exceeding the maximum Total Harmonic Distortion (THD) reported in the EN Standard 50160:2010 is analyzed [23]. In the following subsections, the simulation results are reported and commented separately. In all cases, the sampling frequency is f_s = 5 kHz (i.e., M = 100 samples per nominal cycle are collected) and the final IpD2FT estimation stage relies on a Hann window over observation intervals consisting of C = 2 or C = 4 nominal cycles.

A. Results in noisy M Class testing conditions

The Monte Carlo simulations were repeated 50 times for each testing conditions with the initial phase values changing linearly within [0, 2π]. To model the noise injected by the acquisition stage, a zero-mean, white Gaussian noise with a Signal-to-Noise Ratio (SNR) of 66 dB was added to the signal. This SNR value is in line with the best case measured in high-end experimental setups [24]. The *M Class* testing conditions considered in the study are described below, i.e.

- *Case a*: a static off-nominal frequency deviation ranging from -5 Hz to 5 Hz, including one harmonic at a time from the 2nd to the 50th one with amplitude set to 10% of the fundamental.
- *Case b*: a static off-nominal frequency deviation between -2.5 Hz to 2.5 Hz, with a single OOBI of frequency within [10 Hz, 25 Hz] or [75 Hz, 100 Hz] and amplitude set to 10% of the fundamental.
- *Case c*: sinusoidal amplitude modulation (AM) with 10% modulation index and 5 Hz modulating frequency.
- *Case d:* sinusoidal phase modulation (PM) with 0.1 rad modulation index and 5 Hz modulating frequency.

When the testing conditions labelled as *cases a-d* are considered, the maximum values of Total Vector Error (TVE), absolute Frequency Error (FE) and absolute ROCOF error (RFE) obtained with the WTIpD2FT and the eIpD2FT algorithms for C = 2 and C = 4 are summarized in Table I. The obtained results show that, in most cases, the eIpD2FT

TABLE I –MAXIMUM TVE, |FE| AND |RFE| VALUES OBTAINED WITH THE WTIPD2FT AND THE EIPD2FT ALGORITHMS IN THE M CLASS STEADY-STATE AND DYNAMIC TESTING CONDITIONS SPECIFIED IN THE IEC/IEEE STANDARD 60255-118-1:2018 ASSUMING A NOISE FLOOR WITH SNR=66 dB.

		Max. TVE (%)					Max. |FE| (mHz)					Max. |RFE| (Hz/s)				
Test case		Std. limit	WTIpD2FT		eIpD2FT		Std. limit	WTIpD2FT		eIpD2FT		Std. limit	WTIpD2FT		eIpD2FT	
			C=2	*C*=4	*C*=2	*C*=4		C=2	*C*=4	*C*=2	*C*=4		*C*=2	*C*=4	*C*=2	C=4
a	**±5 Hz Freq. Dev. + one harm. at a time (10%)**	1	0.15	0.03	0.07	0.03	25	0.7	0.03	0.5	0.2	-	0.15	0.003	0.12	0.01
b	**±2.5 Hz Freq. Dev. +10% OOBI**	1.3	3.94	1.70	0.13	0.04	10	201.6	18.2	2.8	0.6	-	35.19	3.09	0.55	0.07
c	**AM (10% @ 5 Hz)**	3	0.51	2.16	0.03	0.03	300	24.3	18.9	0.5	0.2	14	0.69	0.52	0.09	0.03
d	**PM (0.1 rad @ 5 Hz)**	3	0.49	2.03	0.04	0.03	300	49.9	156.0	7.7	30.1	14	1.56	4.81	0.23	0.9

approach outperforms the WTIpD2FT. The performance gap is particularly evident:

- in the presence of OOBIs (especially for *C*=2), because the whitening technique is not able to decorrelate the interferers well enough, when the number of OOBI periods within an observation interval is not integer;
- in the AM and PM tests (especially for *C*=4), because the higher effectiveness of the interferers' whitening technique over longer intervals tends to smooth the modulating tones, thus reducing the tracking capability of the cascaded IpD2FT phasor estimator [6].

The only testing condition in which the WTIpD2FT algorithm performs slightly better than the eIpD2FT one is, when the fundamental is affected by a single 10% harmonic and ±5 Hz frequency deviations over four-cycle-long observation intervals. This behavior is also confirmed by the results shown in Fig. 2, where the maximum TVE, |FE| and |RFE| values obtained with the WTIpD2FTand the eIpD2FT algorithms over *C*=2 or *C*=4 observation intervals, respectively, are plotted as a function of the order of the single harmonic considered. Again, the maxima are computed by increasing the fundamental frequency from 45 Hz to 55 Hz. The bar diagram suggests that when *C*=2, estimating the second harmonic is preferable, whereas when the 3rd and 4th harmonic are considered, the WTIpD2FT algorithm returns lower |FE| and |RFE| values, but higher TVE ones. Over four-cycle-observation intervals instead, both methods return comparable results, but on the whole, the accuracy of the whitening-based algorithm looks slightly better.

B. Results with noise and multiple harmonics

To test and to compare the performance of the two estimation approaches more in depth, further tests were performed under more stressing operating conditions, i.e., including all harmonics from the 2nd to the 7th one (with amplitude set to 2%, 5%, 1%, 6%, 0.5%, and 5% of the fundamental component, respectively) and assuming either a 2-Hz or -3-Hz static frequency offset deviation. Such amplitude and frequency values correspond to the worst-case limits reported in the EN Standard 50160:2010 [23]. As a result, the total Harmonic Distortion (THD) is 9.4%. The tests were repeated for three values of Signal-to-Noise Ratio (SNR), i.e., 40 dB (if the waveforms are collected in a noisy environment), 50 dB (corresponding to a noisy acquisition environment) and 60 dB (i.e., assuming that a high-end experimental setup is used [24]). The maximum TVE, |FE| and |RFE| values obtained with the WTIpD2FT and the eIpD2FT algorithms over two-cycle-long intervals for different frequency offset and SNR values are summarized in Table II.

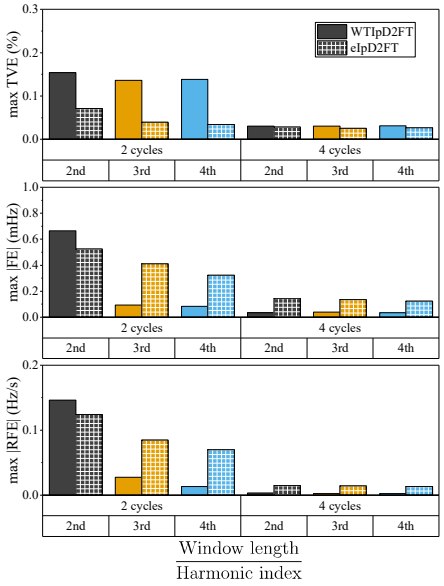

Fig. 2. Maximum TVE, |FE| and |RFE| values obtained with the WTIpD2FTand the eIpD2FT algorithms over *C*=2 or *C*=4 observation lengths, when just the 2nd, the 3rd or the 4th harmonic (all with amplitude equal to 10% of the fundamental) is added to the waveform. The maxima are computed for different frequency offsets between 45 Hz and 55 Hz.

It is worth noting that, unlike the tests with a single harmonic described in Section III.A, in the multi-harmonic case, the whitening-based algorithm returns more accurate estimates of synchrophasor, frequency and ROCOF than the eIpD2FT technique in almost all conditions. This behavior is more evident when the frequency offset is negative, probably due to the slightly longer observation interval resulting from the ESPRIT-based interval adjustment implemented in the WTIpD2FT approach. Quite importantly, the accuracy gap between both algorithms generally grows when the SNR decreases because of the inherent higher sensitivity of the eIpD2FT to wideband noise when the number of parameters to be estimated increases [25]. Indeed, in the case at hand, the eIpD2FT detects all harmonics. Thus, the parameters of seven narrowband components are actually estimated.

IV. CONCLUSIONS

In this paper, two PMU estimation algorithms (called WTIpD2FT and eIpD2FT) are compared to investigate the influence of harmonics and out-of-band interharmonics (OOBIs) on synchrophasor measurements. The WTIpD2FT aims at removing the narrowband interferers through a preliminary two-stage whitening transform, whereas the

TABLE II –MAXIMUM TVE, |FE| AND |RFE| VALUES OBTAINED WITH THE WTIPD2FT AND THE EIPD2FT ALGORITHMS OVER TWO -CYCLE OBSERVATION INTERVALS (C = 2) IN MULTI-HARMONIC TESTS WITH THD = 9.4%, FREQUENCY DEVIATIONS EQUAL TO -3 HZ OR 2 HZ (I.E., THE WORST-CASE LIMITS SPECIFIED IN THE EN STANDARD 50160: 2010) AND DIFFERENT NOISE LEVELS.

		Freq. offset = -3 Hz			Freq. offset = 2 Hz		
		SNR = 40 dB	SNR = 50 dB	SNR = 60 dB	SNR = 40 dB	SNR = 50 dB	SNR = 60 dB
Max. TVE (%)	WTIpD2FT	0.12	0.04	0.03	0.19	0.14	0.14
	eIpD2FT	0.23	0.16	0.12	0.26	0.16	0.12
Max. |FE| (mHz)	WTIpD2FT	2.8	1.6	0.6	2.6	1.5	0.4
	eIpD2FT	6.5	4.9	1.6	9.5	6.4	2.1
Max. |RFE| (Hz/s)	WTIpD2FT	0.67	0.12	0.06	0.71	0.23	0.07
	eIpD2FT	1.28	0.75	0.4	1.78	0.82	0.3

eIpD2FT relies on the singular value decomposition of the same signal autocorrelation matrix to detect the significant narrowband interferers to be included in the signal model. In both cases, the synchrophasor of the fundamental (as well as those of the detected narrowband interferers in the eIpD2FT case), along with the fundamental frequency and ROCOF, are estimated by a final IpD2FT stage. The simulation results in the conditions specified in the IEEE/IEC Standard confirm that estimating the parameters of critical narrowband interferers (especially the OOBIs) is preferable in terms of accuracy. However, when multiple interferers affect the fundamental, the eIpD2FT estimation accuracy is generally worse and it degrades quite faster than the WTIpD2FT one as the wideband noise level grows. Such aspects require a deeper theoretical study that shall be investigated in the future.

ACKNOWLEDGMENT

This work was supported by the Science and Technology Innovation Program of the Hunan Province (Grant no. 2021RC4020) and by the China Research Council.

REFERENCES

[1]. IEC/IEEE 60255-118-1:2018, "IEEE/IEC International Standard - Measuring relays and protection equipment - Part 118-1: Synchrophasor for power systems - Measurements," pp. 1-78, 2018.

[2]. D. Macii and D. Petri, "Digital Filters for Phasor Measurement Units: Design Criteria, Advantages and Limitations," in *2019 IEEE 10th International Workshop on Applied Measurements for Power Systems* (AMPS), 2019, pp. 1-6.

[3]. D. Macii, D. Belega, and D. Petri, "IpDFT-Tuned Estimation Algorithms for PMUs: Overview and Performance Comparison," *Applied Sciences*, vol. 11, no. 5, p. 2318, 2021.

[4]. A. J. Roscoe, I. F. Abdulhadi, and G. M. Burt, "P and M Class Phasor Measurement Unit Algorithms Using Adaptive Cascaded Filters," *IEEE Trans. on Power Delivery*, vol. 28, no. 3, pp. 1447-1459, 2013.

[5]. F. Messina, L. R. Vega, P. Marchi and C. G. Galarza, "Optimal Differentiator Filter Banks for PMUs and Their Feasibility Limits," in *IEEE Trans. on Instrumentation and Measurement*, vol. 66, no. 11, pp. 2948-2956, 2017.

[6]. D. Macii, G. Barchi, and D. Fontanelli, "Decorrelation-based Harmonic Distortion Reduction for Synchrophasor Measurements," in *AMPS 2017 - IEEE International Workshop on Applied Measurements for Power Systems*, Proceedings, Liverpool, UK, 2017.

[7]. A. Bashian, D. Macii, D. Fontanelli and D. Petri, "A Tuned Whitening-Based Taylor-Kalman Filter for P Class Phasor Measurement Units," in *IEEE Trans. on Instrumentation and Measurement*, vol. 71, pp. 1-13, 2022.

[8]. D. Petri, D. Fontanelli, and D. Macii, "A Frequency-Domain Algorithm for Dynamic Synchrophasor and Frequency Estimation," *IEEE Transactions on Instrumentation and Measurement,* vol. 63, no. 10, pp. 2330-2340, 2014.

[9]. M. A. Platas-Garza and J. A. d. l. O. Serna, "Polynomial Implementation of the Taylor–Fourier Transform for Harmonic Analysis," *IEEE Trans. on Instrumentation and Measurement*, vol. 63, no. 12, pp. 2846-2854, 2014.

[10]. J. A. d. l. O. Serna, "Dynamic Phasor Estimates for Power System Oscillations," *IEEE Trans. on Instrumentation and Measurement*, vol. 56, no. 5, pp. 1648-1657, 2007.

[11]. P. Castello, R. Ferrero, P. A. Pegoraro, and S. Toscani, "Space Vector Taylor–Fourier Models for Synchrophasor, Frequency, and ROCOF Measurements in Three-Phase Systems," *IEEE Trans. on Instrumentation and Measurement*, vol. 68, no. 5, pp. 1313-1321, 2019.

[12]. P. Tosato, D. Macii, M. Luiso, D. Brunelli, D. Gallo, and C. Landi, "A Tuned Lightweight Estimation Algorithm for Low-Cost Phasor Measurement Units," *IEEE Transactions on Instrumentation and Measuremen*, vol. 67, no. 5, pp. 1047–1057, 2018,

[13]. Z. D. Drummond, K. E. Claytor, D. R. Allee, and D. M. Hull, "An Optimized Subspace-Based Approach to Synchrophasor Estimation," *IEEE Trans. on Instrumentation and Measurement,* vol. 70, pp. 1-13, 2021.

[14]. J. Song, J. Zhang, and H. Wen, "Accurate Dynamic Phasor Estimation by Matrix Pencil and Taylor Weighted Least Squares Method," *IEEE Trans. on Instrumentation and Measurement,* vol. 70, pp. 1-11, 2021.

[15]. M. Bertocco, G. Frigo, C. Narduzzi, C. Muscas, and P. A. Pegoraro, "Compressive Sensing of a Taylor-Fourier Multifrequency Model for Synchrophasor Estimation," *IEEE Trans. on Instrumentation and Measurement*, vol. 64, no. 12, pp. 3274-3283, 2015.

[16]. G. Frigo, P. A. Pegoraro, and S. Toscani, "Design of Compressive Sensing Adaptive Taylor-Fourier Comb Filters for Harmonic Synchrophasor Estimation," *IEEE Open Journal of Instrumentation and Measurement*, vol. 1, pp. 1-10, 2022.

[17]. A. Derviškadić, P. Romano, and M. Paolone, "Iterative-Interpolated DFT for Synchrophasor Estimation: A Single Algorithm for P- and M-Class Compliant PMUs," *IEEE Trans. on Instrumentation and Measurement,* vol. 67, no. 3, pp. 547-558, 2018.

[18]. X. Shan, D. Macii, D. Petri and H. Wen, "Enhanced IpD2FT-based Synchrophasor Estimation for M Class PMUs through Adaptive Narrowband Interferers Detection and Compensation," in *IEEE Trans. on Instrumentation and Measurement*, vol. 72, 2023.

[19]. M. Wax and T. Kailath, "Detection of Signals by Information Theoretic Criteria," *IEEE Trans. on Acoustics Speech and Signal Processing*, vol. 33, no. 2, pp. 387-392, 1985.

[20]. K. M. Wong, Q. T. Zhang, J. P. Reilly, and P. C. Yip, "On information theoretic criteria for determining the number of signals in high resolution array processing," *IEEE Trans. on Acoustics, Speech, and Signal Processing*, vol. 38, no. 11, pp. 1959-1971, 1990.

[21]. R. Roy and T. Kailath, "ESPRIT-estimation of signal parameters via rotational invariance techniques," *IEEE Transactions on Acoustics, Speech, and Signal Processing*, vol. 37, no. 7, pp. 984-995, 1989.

[22]. S. Kritchman and B. Nadler, "Determining the number of components in a factor model from limited noisy data," *Chemometrics and Intelligent Laboratory Systems*, vol. 94, no. 1, pp. 19-32, Nov 2008.

[23]. EN 50160:2010, *Voltage Characteristics of Electricity Supplied by Public Distribution Systems*, Brussels, Belgium, Dec. 2010.

[24]. M. Luiso, D. Macii, P. Tosato, D. Brunelli, D. Gallo and C. Landi, "A Low-Voltage Measurement Testbed for Metrological Characterization of Algorithms for Phasor Measurement Units," in *IEEE Trans. on Instrumentation and Measurement*, vol. 67, no. 10, pp. 2420-2433, 2018.

[25]. S. M. Kay, *Fundamentals of Statistical Signal Processing: Estimation Theory*, Upper Saddle River, NJ, Prentice Hall, 1997.